Chloride derivatives of lanthanoid(III) *ortho*-oxidotungstates(VI) with the formula *Ln*Cl[WO_4] (*Ln*=Gd–Lu): Syntheses, crystal structures and spectroscopic properties

Tanja Schustereit [a], Thomas Schleid [a], Henning A. Höppe [b], Karolina Kazmierczak [b], Ingo Hartenbach [a,*]

[a] *Institut für Anorganische Chemie, Universität Stuttgart, Pfaffenwaldring 55, 70569 Stuttgart, Germany*
[b] *Institut für Physik, Universität Augsburg, Universitätsstraße 1, 86159 Augsburg, Germany*

1. Introduction

More than 30 years ago, several rare-earth metal(III) chloride oxidotungstates(VI) with the composition *RE*Cl[WO_4] (*RE*=Y, La–Sm [1], Eu–Tm [2]) have been synthesized by Brixner et al. under the aspect of negative thermal expansion materials. The crystal structure of GdCl[WO_4] was determined by X-ray powder diffraction and served further as model for the entire *RE*Cl[WO_4] series with the smaller, but heavier lanthanoids. Now it was possible to synthesize single crystals of the whole sequence of lanthanoid(III) chloride *ortho*-oxidotungstates(VI) with the formula *Ln*Cl[WO_4] for the smaller lanthanoid elements (*Ln*=Gd–Lu) and to analyze structural and spectroscopic details. In the realm of formally analogous rare-earth metal(III) chloride oxidomolybdates(VI) *RE*Cl[MoO_4] with *RE*=Y, Sm–Lu [3,4], as obvious close relatives of the respective tungstates, a structural gap within the *Ln*Cl[MoO_4] series for the smaller lanthanoids can be detected between ytterbium and lutetium [4]. The representatives of these molybdates from gadolinium to ytterbium crystallize monoclinically, thus isotypically to the monoclinic structure of the respective chloride oxidotungstates in the present paper. However, the structural gap for the latter is here situated between erbium and thulium. This contradicts to the statement of Brixner, who claims the whole *Ln*Cl[WO_4] series from europium to thulium to be monoclinic [2]. Furthermore, EuCl[WO_4] is found to be at least dimorphic, since it crystallizes in the structure type of the smaller lanthanoids [1] as well as in the structure type of the larger ones [5,6]. As the respective oxidomolybdates, oxidotungstates are also known to exhibit $O^{2-} \rightarrow M^{6+}$ charge transfer bands upon excitation with UV light (maximum at about 290 nm [7] for both regarded units). This energy can be harvested to excite luminescence-active Ln^{3+} cations, such as Eu^{3+} and Tb^{3+} [7], hence an inorganic antenna effect [8] based on tetrahedral $[MO_4]^{2-}$ anions (*M*=Mo and W) is present in these structures. Although soft anions like Cl^- sometimes cause severe luminescence quenching [3], both

* Corresponding author. Fax: +49 711 685 54254.
E-mail address: hartenbach@iac.uni-stuttgart.de (I. Hartenbach).

structure types of the *Ln*Cl[WO_4] series with *Ln*=Gd–Lu have proven to be suitable host lattices with optically innocent Ln^{3+} cations (*Ln*=Gd and Lu) for delivering luminous performance when doped with the aforementioned active trications. While the luminescence properties of rare-earth metal oxidotungstates are widely investigated, e.g. in terms of luminescence optimization [9], upconversion [10] etc., their halide derivatives remain carelessly overlooked, which is partly remedied in this paper.

2. Experimental

2.1. Synthesis

The lanthanoid(III) chloride *ortho*-oxidotungstates(VI) with the formula *Ln*Cl[WO_4] were obtained by solid-state reactions involving mixtures of the respective lanthanoid sesquioxides (Gd_2O_3, Dy_2O_3, Ho_2O_3, Tm_2O_3: all 99.9%; ChemPur, Karlsruhe, Germany; Er_2O_3, Yb_2O_3: both 99.9%; Auer-Remy GmbH, Hamburg, Germany; Lu_2O_3: 99.9%, Heraeus, Hanau, Germany), the corresponding lanthanoid trichlorides ($GdCl_3$, $TbCl_3$, $DyCl_3$, $ErCl_3$, $LuCl_3$: all 99.9%; Heraeus, Hanau, Germany; $HoCl_3$: 99.9%; Alfa Aesar, Karlsruhe, Germany; $TmCl_3$, $YbCl_3$: both 99.9%; ChemPur, Karlsruhe, Germany), and tungsten trioxide (WO_3: p.a.; Merck, Darmstadt, Germany) with Ln_2O_3:*Ln*Cl_3:WO_3 in molar ratios of 1:5:3. The reactions took place in evacuated, fused silica ampoules by heating for seven days at 950 °C according to Eq. (1). *Ln*Cl_3 was used as reactand and flux simultaneously with a fivefold excess, which could be readily removed from the bulk by washing with water.

$$Ln_2O_3 + LnCl_3 + 3WO_3 \rightarrow 3LnCl[WO_4] \quad (1)$$

Since Tb_2O_3 is not available from commercial sources, this oxide has to be produced in situ by synproportionation of elemental terbium (99.9%; ChemPur, Karlsruhe, Germany) and the appropriate amount of Tb_4O_7 (99.9%; ChemPur, Karlsruhe, Germany) according to Eq. (2).

$$Tb + 3Tb_4O_7 \rightarrow 7Tb_2O_3 \quad (2)$$

During all reactions transparent, lath shaped single crystals were obtained, which remained stable to environmental conditions and displayed the typical color of the respective lanthanoid trication (colorless for *Ln*=Gd, Tb, Yb, Lu; pale green for *Ln*=Dy, Tm; yellow for *Ln*=Ho; pink for *Ln*=Er). For the synthesis of the Eu^{3+}-doped samples 1% of the respective rare-earth metal sesquioxide was substituted with Eu_2O_3 (99.9%; ChemPur, Karlsruhe, Germany).

2.2. X-ray powder diffraction

The high melting temperature of tungsten trioxide (WO_3) at 1473 °C provides a difficulty for the synthesis of lanthanoid(III) chloride *ortho*-oxidotungstates(VI) by solid-state methods, but could be overcome by using an excess of the respective lanthanoid trichloride *Ln*Cl_3 as flux in order to lower the reaction temperature to 950 °C. The X-ray powder patterns (Figs. 1 and 2) show that the flux was completely removed from the crystals of the title compounds by washing the crude products with water and phase-pure monoclinic or triclinic compounds could be obtained. Despite the relatively high reaction temperature, no silicate-containing by-products were identified in the XRD patterns, which is rather uncommon after reactions of tungsten oxides and halide compounds in fused silica ampoules.

Intensity data sets for powders of all representatives within the *Ln*Cl[WO_4] series (*Ln*=Gd–Lu) were collected on a STADI P diffractometer (Stoe & Cie) using germanium-monochromatized Cu-*K*α radiation (wavelength: λ=154.06 pm). Further processing

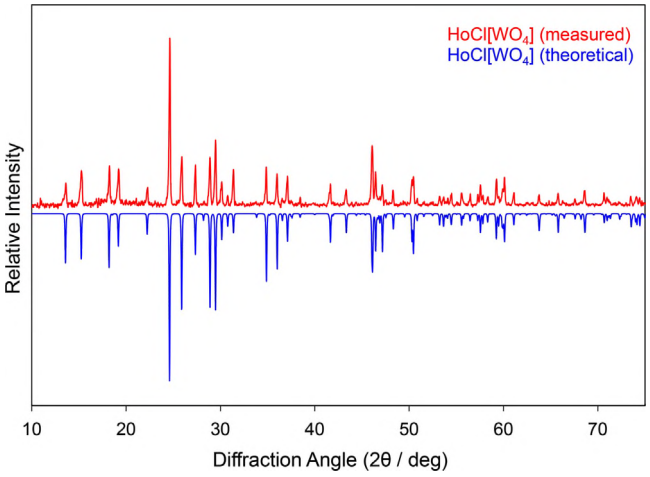

Fig. 1. X-ray powder diffraction pattern of HoCl[WO_4] as example for the structures of the monoclinic *Ln*Cl[WO_4] series with *Ln*=Gd–Er.

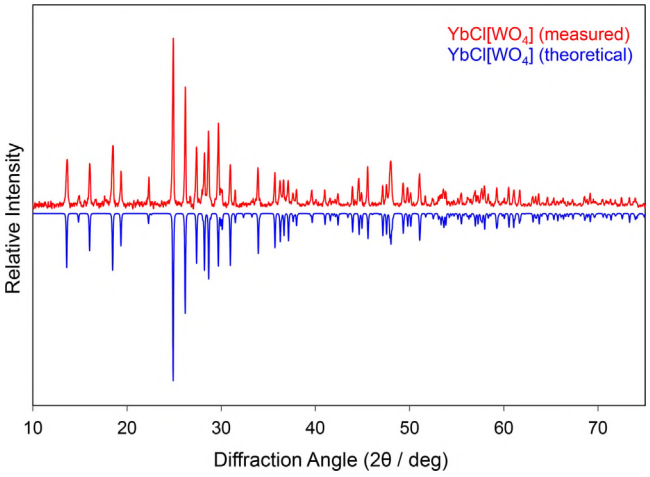

Fig. 2. X-ray powder diffraction pattern of YbCl[WO_4] as example for the structures of the triclinic *Ln*Cl[WO_4] series with *Ln*=Tm–Lu.

of the collected data was carried out with the program STOE WinXpow 3.04 [11] in all cases.

2.3. X-ray crystallography

Intensity data sets for all single crystals of the *Ln*Cl[WO_4] series (*Ln*=Gd–Lu) were collected on a Nonius Kappa-CCD diffractometer using graphite-monochromatized Mo-*K*α radiation (wavelength: λ=71.07 pm). Numerical absorption correction was performed with the program Habitus [12] in all cases. The crystal structure solutions and refinements were carried out utilizing the program package Shelx-2013 [13]. Details of the data collections and structure refinements [14] are summarized in Tables 1 and 2, the motifs of mutual adjunction [15–18] can be found in Tables 3 and 4, selected interatomic distances and angles are given in Tables 5 and 6. Further details of the crystal structure investigations are available from the Fachinformationszentrum (FIZ) Karlsruhe, D-76344 Eggenstein-Leopoldshafen, Germany (Fax: +49 7247 808 666; E-mail: crysdata@fiz-karlsruhe.de), upon citing the respective CSD-numbers from Tables 1 and 2.

2.4. Single-crystal Raman spectroscopy

Single-crystal Raman spectroscopy for TbCl[WO_4] as example for the monoclinic structures of the *Ln*Cl[WO_4] series with *Ln*=Gd–Er and for YbCl[WO_4] as example for the triclinic structures of the

Table 1
Crystallographic data for the monoclinic *Ln*Cl[WO_4] representatives with *Ln*=Gd–Er.

***Ln*=**	**Gd**	**Tb**	**Dy**	**Ho**	**Er**
Crystal system, formula units, space group	Monoclinic, $Z=4$ $C2/m$, (no. 12)				
Lattice parameters, a (pm)	1032.19(5)	1028.06(5)	1025.24(5)	1021.54(5)	1018.77(5)
b (pm)	732.49(3)	728.58(3)	725.83(3)	723.03(3)	720.53(3)
c (pm)	688.88(3)	687.13(3)	685.61(3)	683.33(3)	68.201(3)
β (°)	107.229(2)	107.293(2)	107.401(2)	107.470(2)	107.561(2)
Calculated density, D_x (g cm^{-3})	5.882	5.977	6.082	6.184	6.270
Molar volume, V_m (cm^3 mol^{-1})	74.89	73.98	73.30	72.48	71.86
F(000)	748	752	756	760	764
Index range, $\pm h/\pm k/\pm l$	13/9/9	14/10/9	14/10/9	14/10/9	13/9/9
Theta range, θ_{min}–θ_{max}	3.1–28.0	3.1–30.5	3.1–30.5	3.1–30.5	3.1–25.2
Absorption coefficient, μ (mm^{-1})	36.75	38.10	39.28	40.64	41.99
Data corrections	Background, polarization and Lorentz factors, numerical absorption correction with the program *HABITUS* [12]				
Refined parameters	41				
Number of reflections, collected/unique	7000/649	8316/805	7588/797	7239/791	7052/642
R_{int}/R_σ	0.083/0.030	0.083/0.030	0.078/0.031	0.103/0.037	0.110/0.038
Structure solution and refinement	Program package *SHELX-2013* [13], scattering factors according to International Tables, Vol. C [14]				
R_1 for (n) reflections with $\|F_o\| \geq 4\sigma(F_o)$	0.020 (621)	0.026 (790)	0.021 (726)	0.024 (769)	0.022 (617)
R_1/wR_2 for all reflections	0.021/0.048	0.026/0.066	0.025/0.051	0.024/0.059	0.023/0.054
Goodness of Fit (GooF)	1.058	1.097	1.040	1.127	1.087
Extinction, g	0.0401 (9)	0.0453 (12)	0.0037 (2)	0.0135 (4)	0.0299 (8)
Residual electron density, ρ/e$^-$ • 10^{-6} pm^{-3}, min./max.	−1.55/1.90	−2.26/3.15	−1.75/3.05	−2.35/2.43	−1.84/2.03
CSD numbers	427661	425496	427662	427663	427664

Table 2
Crystallographic data for the triclinic *Ln*Cl[WO_4] representatives with *Ln*=Tm–Lu.

***Ln*=**	**Tm**	**Yb**	**Lu**
Crystal, system formula units, space group	Triclinic $Z=2$ $P\bar{1}$ (no. 2)		
Lattice parameters, a (pm)	596.38(3)	592.35(3)	592.92(3)
b (pm)	721.10(4)	718.45(4)	718.69(4)
c (pm)	685.51(4)	684.48(4)	684.43(4)
α (°)	93.243(3)	93.523(3)	93.637(3)
β (°)	103.066(3)	103.001(3)	102.994(3)
γ (°)	121.995(3)	121.745(3)	121.875(3)
Calculated density, D_x (g cm^{-3})	6.312	6.432	6.463
Molar volume, V_m (cm^3 mol^{-1})	71.64	70.95	70.91
F(000)	384	386	388
Index range, $\pm h/\pm k/\pm l$	8/10/9	8/10/10	8/10/9
Theta range, θ_{min}–θ_{max}	3.1–25.2	3.1–25.2	3.1–30.2
Absorption coefficient, μ (mm^{-1})	43.13	44.57	45.70
Data corrections	Background, polarization and Lorentz factors, numerical absorption correction by the program *HABITUS* [12]		
Refined parameters	65		
Number of reflections, collected/unique	10,072/1,401	12,249/1,649	8907/1394
R_{int}/R_σ	0.118/ 0.057	0.098/ 0.042	0.097/ 0.045
Structure solution and refinement	Program package *SHELX-2013* [13], scattering factors according to International Tables, Vol. C [14]		
R_1 for (n) reflections with $\|F_o\| \geq 4\sigma(F_o)$	0.037 (1236)	0.036 (1589)	0.033 (1278)
R_1/wR_2 for all reflections	0.042/0.097	0.037/0.094	0.036/0.081
Goodness of Fit (GooF)	1.015	1.103	1.050
Extinction, g	0.037 (2)	0.017 (1)	0.0052 (6)
Residual electron density, ρ/e$^-$ • 10^{-6} pm^{-3}, min./max.	−3.00/2.81	−3.74/5.40	−2.22/4.61
CSD numbers	427665	427666	427667

Table 3
Motifs of mutual adjunction [15–18] for the monoclinic *Ln*Cl[WO_4] representatives with *Ln*=Gd–Er.

	Cl	**O1**	**O2**	**O3**	**CN**
Ln	2/2	1/1	1/1	4/2	8
W	0/0	1/1	1/1	2/1	4
CN	2	2	2	3	

Table 4
Motifs of mutual adjunction [15–18] for the triclinic *Ln*Cl[WO_4] representatives with *Ln*=Tm–Lu.

	Cl	**O1**	**O2**	**O3**	**O4**	**CN**
Ln	2/2	1/1	1/1	1/1	2/1	7
W	0/0	1/1	1/1	1/1	1/1	4
CN	2	2	2	2	2	

*Ln*Cl[WO_4] series with *Ln*=Tm–Lu was performed with the help of a Horiba XploRa spectrometer using a LASER device with a wavelength of λ=638 nm (TbCl[WO_4]) or 532 nm (YbCl[WO_4]) for irradiation of the single crystals, respectively.

2.5. Diffuse reflectance spectroscopy

The diffuse reflectance spectrum (DRS) for TbCl[WO_4] as example for the monoclinic structures of the *Ln*Cl[WO_4] series

with *Ln*=Gd–Er and the spectrum for YbCl[WO_4] as example for the triclinic structures of the *Ln*Cl[WO_4] series with *Ln*=Tm–Lu were taken from the finely powdered bulk substances and have been recorded with a J&M TIDAS UV–vis–NIR spectrophotometer equipped with accessory to measure diffuse reflection. Barium sulfate ($BaSO_4$) was used as standard white reference and the *Kubelka–Munk* function was applied to obtain band-gap information [19–21].

Table 5
Selected interatomic distances (*d*/pm) and bond angles (∢/deg) for the monoclinic *Ln*Cl[WO_4] representatives with *Ln*=Gd–Er.

***Ln*=**	**Gd**	**Tb**	**Dy**	**Ho**	**Er**
Ln–O1 (1x)	234.7(6)	232.7(6)	230.9(5)	228.6(6)	230.6(6)
Ln–O2 (1x)	233.1(5)	231.5(6)	231.2(6)	229.0(5)	228.8(5)
Ln–O3 (2x)	232.6(3)	229.8(3)	228.8(3)	227.2(4)	226.3(4)
Ln–O3′ (2x)	262.9(3)	262.6(4)	261.9(4)	260.5(4)	261.2(4)
Ln–Cl (1x)	273.2(2)	272.1(2)	270.3(2)	269.7(2)	268.3(2)
Ln–Cl′ (1x)	277.3(2)	276.0(2)	274.9(2)	273.7(2)	272.8(2)
W–O1 (1x)	173.1(6)	173.9(6)	175.9(5)	175.6(6)	172.7(6)
W–O2 (1x)	176.6(5)	176.4(6)	174.4(6)	176.2(6)	175.1(5)
W–O3 (2x)	178.7(3)	179.5(4)	179.1(3)	179.6(4)	178.6(3)
O1–W–O2 (1x)	109.9(2)	110.3(3)	109.7(3)	109.9(3)	110.6(3)
O1–W–O3 (2x)	111.6(1)	114.3(2)	111.2(2)	111.7(2)	111.0(2)
O2–W–O3 (2x)	111.4(1)	111.3(2)	111.9(2)	111.4(2)	111.5(2)
O3–W–O3 (1x)	116.9(2)	100.8(2)	100.7(2)	100.4(2)	101.0(2)

Table 6
Selected interatomic distances (*d*/pm) and bond angles (∢/deg) for the triclinic *Ln*Cl[WO_4] representatives with *Ln*=Tm–Lu.

***Ln*=**	**Tm**	**Yb**	**Lu**
Ln–O1 (1x)	225.4(6)	224.3(6)	223.6(7)
Ln–O2 (1x)	229.1(6)	226.3(6)	224.6(7)
Ln–O3 (1x)	222.3(6)	222.1(6)	223.3(7)
Ln–O4 (1x)	225.3(6)	224.5(6)	222.3(6)
Ln–O4′ (1x)	239.8(6)	237.6(6)	236.9(6)
Ln–Cl (1x)	270.0(2)	268.8(2)	268.4(2)
Ln–Cl′ (1x)	270.0(2)	269.4(2)	269.3(3)
W–O1 (1x)	174.7(6)	174.7(6)	175.1(7)
W–O2 (1x)	174.5(6)	176.1(7)	176.9(7)
W–O3 (1x)	178.4(6)	177.4(6)	176.3(7)
W–O4 (1x)	181.9(6)	181.6(6)	184.1(7)
O1–W–O2 (1x)	108.9(3)	108.9(3)	109.0(3)
O1–W–O3 (1x)	109.9(3)	110.0(3)	109.5(3)
O1–W–O4 (1x)	111.2(3)	110.9(3)	110.9(3)
O2–W–O3 (1x)	109.9(3)	109.9(3)	110.0(3)
O2–W–O4 (1x)	112.3(3)	112.8(3)	112.7(3)
O3–W–O4 (1x)	104.5(3)	104.2(3)	104.7(3)

2.6. Luminescence spectroscopy

Solid-state excitation and emission spectra of GdCl[WO_4]:Eu^{3+}, LuCl[WO_4]:Eu^{3+}, and bulk TbCl[WO_4] were recorded at room temperature using a Horiba FluoroMax-4 fluorescence spectrometer equipped with a xenon discharge lamp scanning a range from 200 to 800 nm. Electronic transitions were assigned according to the energy-level diagrams of the trivalent europium and terbium cations, respectively [22].

3. Results and discussion

3.1. Crystal structures

The members of the *Ln*Cl[WO_4] series crystallize monoclinically in space group *C*2/*m* (*a*=1019–1032, *b*=721–733, *c*=682–689 pm and *β*=107–108°, *Z*=4, Table 1) with *Ln*=Gd–Er and triclinically in space group *P*1 (*a*=593–596, *b*=719–721, *c*=684–686 pm, α=93–94, *β*≈103 and *γ*≈122°, *Z*=2, Table 2) with *Ln*=Tm–Lu. The monoclinic crystal structure of the *Ln*Cl[WO_4] representatives for *Ln*=Gd–Er is not only isostructural with the one described for GdCl[WO_4] by Brixner et al. [2], but also with the most examples of the formally analogous rare-earth metal(III) chloride oxidomolybdates(VI) *RE*Cl[MoO_4] with yttrium and the smaller lanthanoids (*RE*=Y, Sm–Yb) [3,4]. The structure contains crystallographically unique Ln^{3+} cations, which are surrounded by two Cl^- and six O^{2-} anions (CN=8, Table 3) forming a distorted trigonal dodecahedron (Fig. 3, left). The triclinic crystal structure of the *Ln*Cl[WO_4] representatives for *Ln*=Tm–Lu is isotypic with the formally analogous lutetium(III) chloride oxidomolybdate(VI) LuCl[MoO_4] [4]. The slightly distorted monocapped trigonal prisms around the crystallographically unique Ln^{3+} cations (Fig. 3, right) are also built up by two Cl^-, but only five O^{2-} anions (CN=7, Table 4). The distances between the lanthanoid(III) cations and the oxide anions of 226–263 pm for *Ln*=Gd–Er and 222–240 pm for *Ln*=Tm–Lu as well as those between the Ln^{3+} cations and the Cl^- anions with values of 268–277 pm for *Ln*=Gd–Er and 268–270 pm for *Ln*=Tm–Lu (Tables 5 and 6) are situated well in the range of the respective binary C-type sesquioxides (e.g. Gd_2O_3: $d(Gd^{3+}–O^{2-})$=224–262 pm, Lu_2O_3: $d(Lu^{3+}–O^{2-})$=215–251 pm [23]) and some ternary or quaternary chloride-containing compounds (e.g. $Gd_6Cl_{10}[Si_4O_{12}]$: $d(Gd^{3+}–Cl^-)$=266–288 pm [24], $Cs_3Lu_2Cl_9$: $d(Lu^{3+}–Cl^-)$=250–270 pm [25]).

For the monoclinic crystal structure of the *Ln*Cl[WO_4] representatives with *Ln*=Gd–Er, these polyhedra are fused together via three common edges consisting of four oxide and two chloride anions, respectively, to form anionic $^2_\infty\{[LnCl^e_{2/2}O^e_{4/2}O^t_{2/1}]^{6-}\}$ layers (*e*=edge-sharing, *t*=terminal), parallel to the *ab* plane (Fig. 4, top).

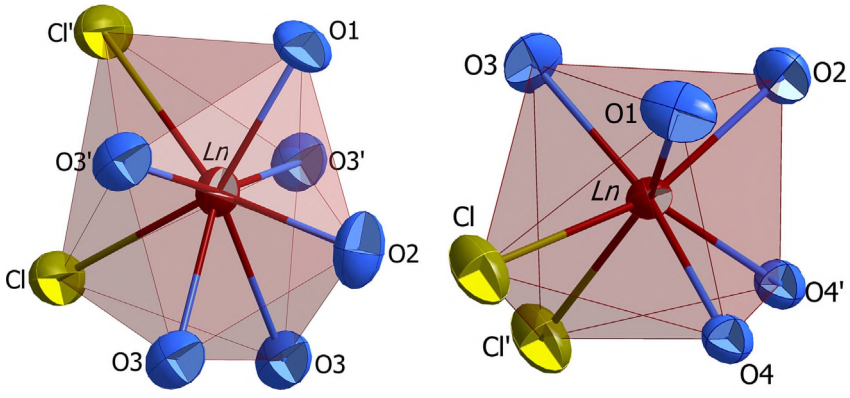

Fig. 3. Coordination polyhedra around the Ln^{3+} cations (ellipsoid representation at 95%) for *Ln*=Gd–Er (monoclinic, left) and *Ln*=Tm–Lu (triclinic, right) in the crystal structures of the *Ln*Cl[WO_4] series with *Ln*=Gd–Lu.

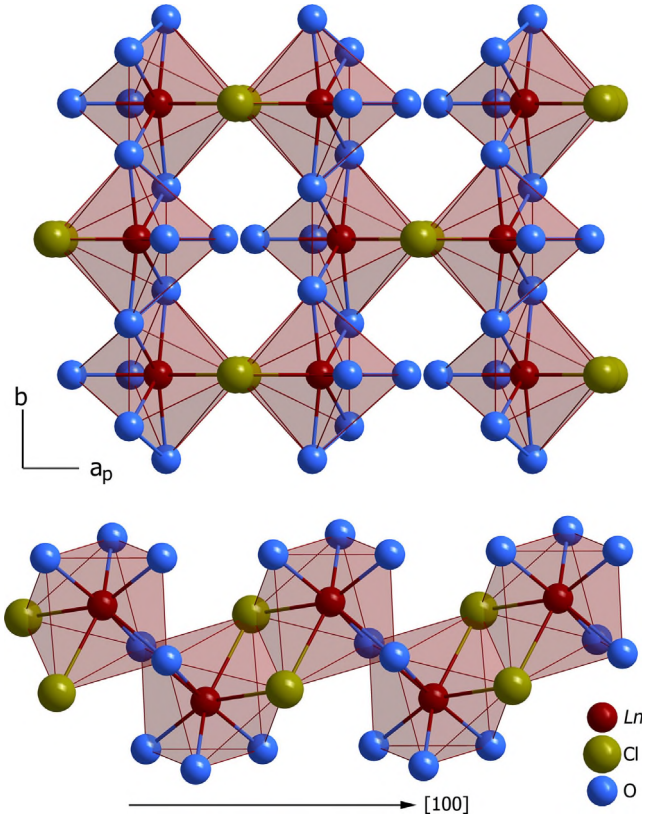

Fig. 4. View at the $^{2}_{\infty}\{[LnCl^{e}_{2/2}O^{e}_{4/2}O^{t}_{2/1}]^{6-}\}$ layers parallel to (001) for *Ln*=Gd–Er (monoclinic, top) and the $^{1}_{\infty}\{[LnCl^{e}_{2/2}O^{e}_{2/2}O^{t}_{3/1}]^{6-}\}$ strands along [100] for *Ln*=Tm–Lu (triclinic, bottom) in the crystal structures of the *Ln*Cl[WO_4] series.

The monocapped trigonal prisms as coordination polyhedra around the Ln^{3+} cations within the triclinic structure of the *Ln*Cl[WO_4] representatives with *Ln*=Tm–Lu are interconnected via one chloride, but only one more oxide edge, which leads to anionic $^{1}_{\infty}\{[LnCl^{e}_{2/2}O^{e}_{2/2}O^{t}_{3/1}]^{6-}\}$ strands running along the [100] direction (Fig. 4, bottom).

Finally, both the $^{2}_{\infty}\{[LnCl^{e}_{2/2}O^{e}_{4/2}O^{t}_{2/1}]^{6-}\}$ layers and the $^{1}_{\infty}\{[LnCl^{e}_{2/2}O^{e}_{2/2}O^{t}_{3/1}]^{6-}\}$ strands within the two structure types become interconnected by W^{6+} cations to build up the complete structures by generating discrete $[WO_4]^{2-}$ tetrahedra (Fig. 5).

The distances between the W^{6+} cations and the four O^{2-} anions ($d(W^{6+}–O^{2-})$=173–184 pm) within the isolated $[WO_4]^{2-}$ units are in a good agreement with those found in other lanthanoid(III) oxidotungstates(VI) (e.g. $La_2[WO_4]_3$: $d(W^{6+}–O^{2-})$=171–187 pm [26]). Their W–O–W bond angles range from 100 to 114° (Tables 5 and 6), thus showing a deviation of the ideal tetrahedral angle (109.5°) by about 9%. In the monoclinic structure the smallest angle of 100° results from the only edge-connection of the $[WO_4]^{2-}$ anions to the Ln^{3+} cations, whereas this deviation is considerably less distinct in the triclinic compounds, in which the only edge-capping contact to Ln^{3+} loses one of its connection points to the $[WO_4]^{2-}$ tetrahedra and remains just as a vertex-connecting function (Fig. 6).

3.2. Single-crystal Raman spectroscopy

In the crystal structure of the monoclinic phases, the tetrahedral $[WO_4]^{2-}$ units exhibit the point symmetry *m*, while for the triclinic ones the point symmetry is just 1. For both of these symmetries five stretching vibrations and four deformation modes are visible in the respective Raman spectrum [27]. In the spectra of the monoclinic and triclinic compounds the strongest peaks represent the total symmetric stretching vibration, which is also located at higher

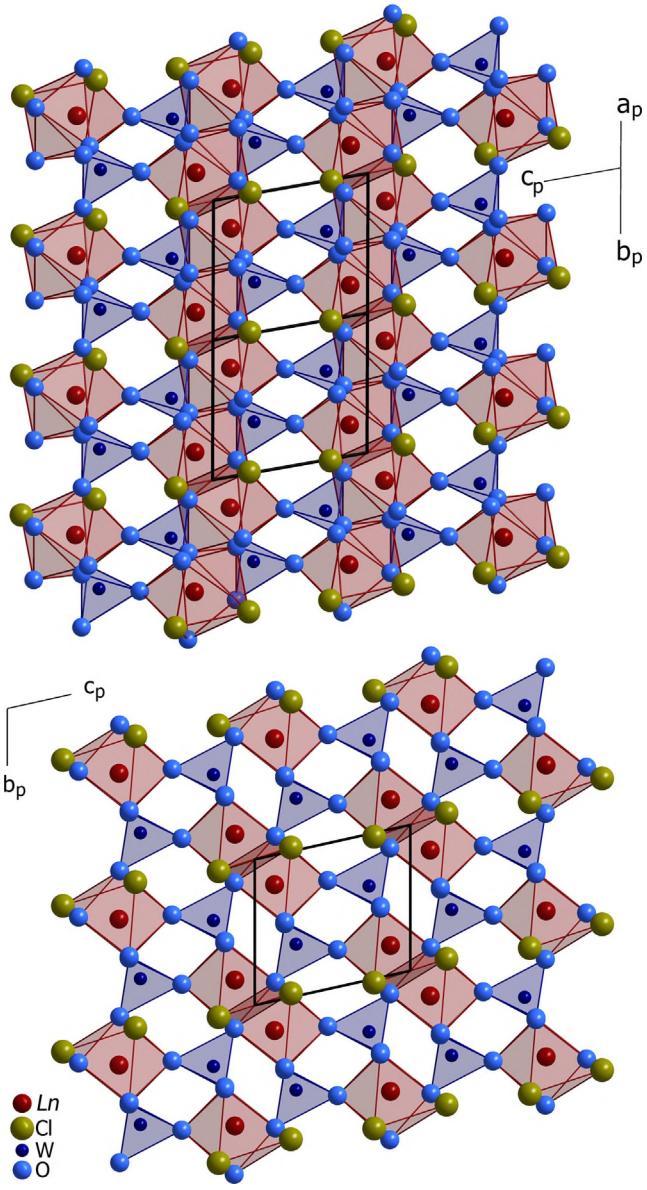

Fig. 5. View at the crystal structures of the *Ln*Cl[WO_4] series along the [110] direction for *Ln*=Gd–Er (monoclinic, top) and along the [100] direction for *Ln*=Tm–Lu (triclinic, bottom).

energy than the three asymmetric ones in the range from 800 to 900 cm^{-1}. The spectrum of TbCl[WO_4] exhibits the symmetric mode at 990 cm^{-1} and the spectrum of YbCl[WO_4] at 991 cm^{-1} (Fig. 7). These band positions are in good agreement with those found in the literature for perfectly isolated $[WO_4]^{2-}$ tetrahedra at 931 cm^{-1} [27]. The remaining three asymmetric stretching vibrations between 760 and 900 cm^{-1} wavenumbers emerge as well resolved peaks for the triclinic compounds, while for the monoclinic ones the peaks at wavenumbers 835 and 863 cm^{-1} could be allocated as two of the three asymmetric modes, which are well resolved with the third one at 820 cm^{-1} being almost invisible. The lower peaks in the region of 300–450 cm^{-1} could be identified as resulting from Ln^{3+}–O^{2-} stretching vibrations as well as deformation modes of the $[WO_4]^{2-}$ tetrahedra for both structure types. The results for TbCl[WO_4] were obtained with a LASER wavelength of λ=638 nm and due to fluorescent overlays at this wavelength for YbCl[WO_4] the corresponding measurements have been carried out at a lower wavelength of λ=532 nm.

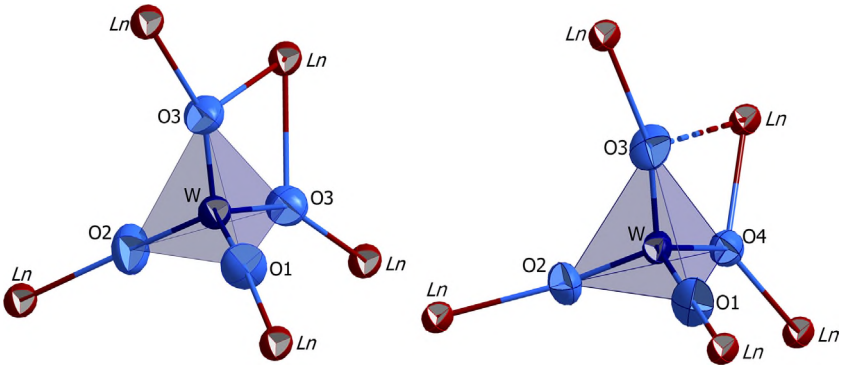

Fig. 6. Cationic coordination environment around the $[WO_4]^{2-}$ anions (ellipsoid representation at 95%) for *Ln*=Gd–Er (monoclinic, left) and *Ln*=Tm–Lu (triclinic, right) in the crystal structures of the *Ln*Cl[WO_4] series with *Ln*=Gd–Lu.

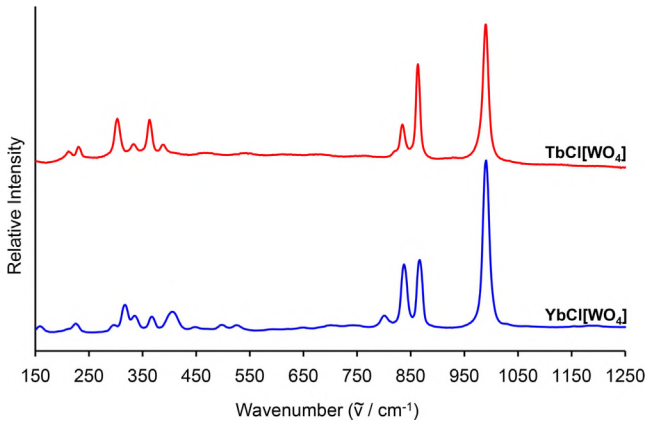

Fig. 7. Single-crystal Raman spectra of monoclinic TbCl[WO_4] (top) and triclinic YbCl[WO_4] (bottom) as examples for both different representatives of the *Ln*Cl[WO_4] series with *Ln*=Gd–Lu.

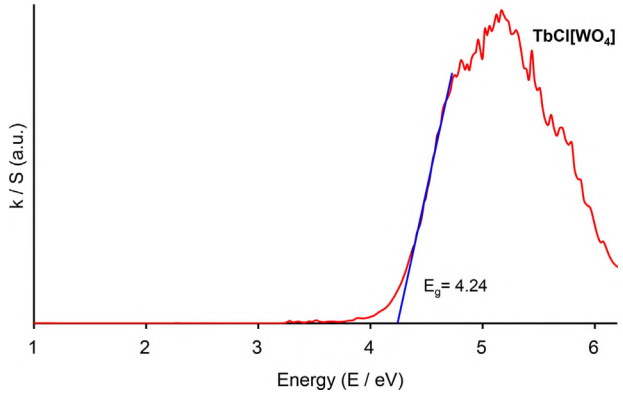

Fig. 8. Diffuse reflectance spectrum (DRS) of monoclinic TbCl[WO_4] as example for the structures of the *Ln*Cl[WO_4] series with *Ln*=Gd–Er with linear adjustment.

3.3. Diffuse reflectance spectroscopy

Diffuse reflectance spectra (DRS) of the chloride oxidotungstates(VI) were taken from finely powdered bulk substances. The spectrum of TbCl[WO_4] shows an optical band gap of 4.24 eV, which is situated at 292 nm in the UV range of the electromagnetic spectrum (Fig. 8), while the band gap of YbCl[WO_4] was determined to be 4.23 eV (293 nm, Fig. 9). In the presented compounds, the band gaps are about 20% lower than those found in materials comprising two complex anions, such as $Na_2Y[PO_4][WO_4]$ with a band gap of 5.1 eV [28]. Besides these band gaps, the *f*–*f* transitions of the Tb^{3+} cations are barely visible between 3.2 and 4.2 eV. The

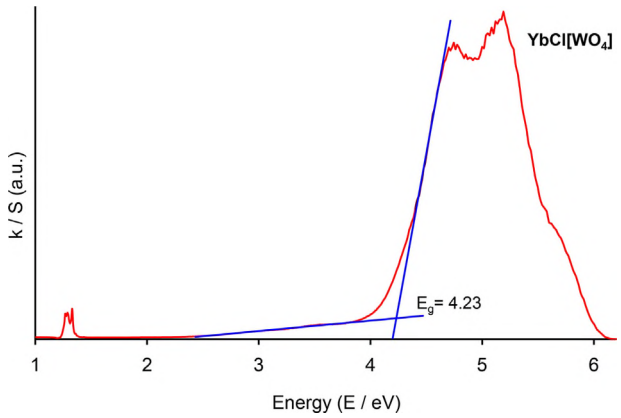

Fig. 9. Diffuse reflectance spectrum (DRS) of triclinic YbCl[WO_4] as example for the structures of the *Ln*Cl[WO_4] series with *Ln*=Tm–Lu with linear adjustment.

f–*f* transitions ($^2F_{7/2}\rightarrow{}^2F_{5/2}$) of the Yb^{3+} cations, however, can be clearly allocated at 1.3 eV, also agreeing well with the literature values [22,29].

3.4. Luminescence spectroscopy

Bulk luminescence of europium- or terbium-containing compounds has been observed for chloride oxidomolybdates(VI) with the formula *RE*Cl[MoO_4] (*RE*=Eu and Tb) [4], while doping experiments with Eu^{3+} or Tb^{3+} cations in rare-earth metal(III) chloride *ortho*-oxidomolybdates (e.g. YCl[MoO_4] [3]) did not yield luminescent materials in contrast to the isotypic tungstates. As the undoped materials GdCl[WO_4] and LuCl[WO_4] show the white charge-transfer luminescence of the tetrahedral $[WO_4]^{2-}$ group under UV excitation at 254 nm, an intense red luminescence is observed for GdCl[WO_4]:Eu^{3+} and LuCl[WO_4]:Eu^{3+} upon excitation at λ=366 nm. In the excitation spectra of the aforementioned compounds as well as TbCl[WO_4] (Figs. 10–12, left curves), a wide band around 290 nm appears, which can be attributed to the $O^{2-}\rightarrow W^{6+}$ **l**igand-to-**m**etal **c**harge **t**ransfer (LMCT) effect, which is quite typical for structures containing isolated $[WO_4]^{2-}$ anions [30]. The emission of these units occurs at about 500 nm, but for TbCl[WO_4] and the Eu^{3+}-doped materials the corresponding signals in the emission spectra are superimposed by stronger effects caused by the luminescence-active lanthanoid(III) cations. In TbCl[WO_4], the Tb^{3+} cations are situated at the *Wyckoff* position 4*i*, which implies a mirror plane, but no inversion center. Hence, the electric dipole transition $^5D_4\rightarrow{}^7F_5$ could be identified as strongest peak of the emission spectrum at 545 nm and the magnetic dipole transition $^5D_4\rightarrow{}^7F_6$ is assigned to the considerably weaker peak at 488 nm in the emission spectrum [22] (right curve in Fig. 10).

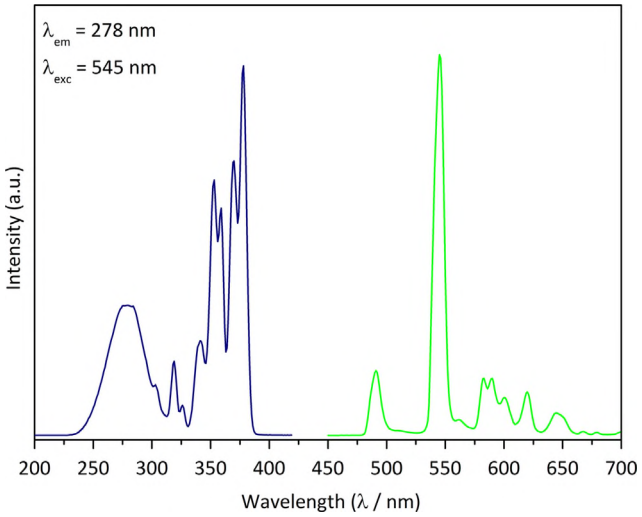

Fig. 10. Excitation (left) and emission spectrum (right) of bulk $TbCl[WO_4]$.

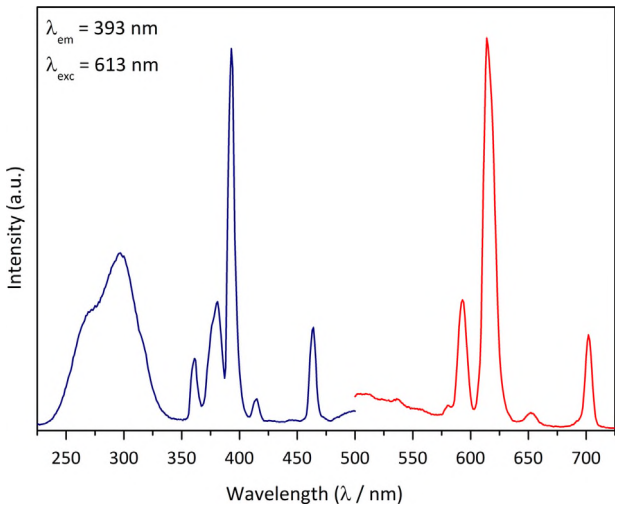

Fig. 12. Excitation (left) and emission spectrum (right) of $LuCl[WO_4]:Eu^{3+}$.

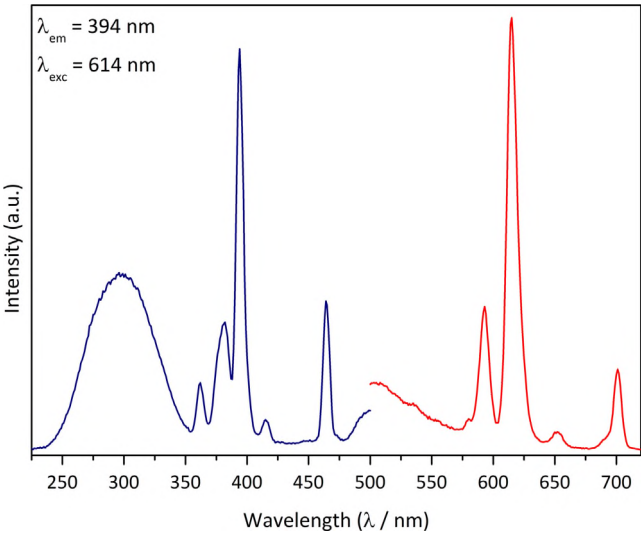

Fig. 11. Excitation (left) and emission spectrum (right) of $GdCl[WO_4]:Eu^{3+}$.

The same is true for the emission spectra of the Eu^{3+} cations substituting the Gd^{3+} sites in the isotypic structure of $GdCl[WO_4]:Eu^{3+}$, where the electric dipole transition $^5D_0 \rightarrow {}^7F_2$ is superior to the magnetic dipole transition $^5D_0 \rightarrow {}^7F_1$ [22] (Fig. 11, right curve). In $LuCl[WO_4]:Eu^{3+}$ the situation is basically analogous with the luminescence-active Eu^{3+} cations at the *non*-centrosymmetric *Wyckoff* position 2*i* (Fig. 12, right curve).

Comparing both Eu^{3+}-doped compounds, a significantly different cationic environment around the Ln^{3+} cations is found, but the LMCT peak in the excitation spectra remains basically in the same range. Therefore, the $O^{2-} \rightarrow Eu^{3+}$ charge-transfer process, which usually also plays an important role regarding LMCT transitions, gives obviously an inferior contribution to the overall charge-transfer energy range in the competition with the $O^{2-} \rightarrow W^{6+}$ LMCT transition.

4. Conclusion

In this publication the synthesis and crystal structures of the lanthanoid(III) chloride *ortho*-oxidotungstates(VI) with the formula $LnCl[WO_4]$ (Ln=Gd–Lu) are described, and structural misconceptions in the series of the $LnCl[WO_4]$ representatives with Ln=Gd–Lu could be clarified for the first time based on single-crystal X-ray diffraction data. All products of this series were synthesized as single-phase samples, proven by X-ray powder diffraction (XRD). Spectroscopic measurements have been carried out for selected examples and luminescence spectra of both bulk Tb^{3+}-containing and Eu^{3+}-doped materials could be recorded, despite the fact that compounds containing soft anions such as Cl^- usually exhibit luminescence quenching. The facile synthesis with easy-to-handle chemicals leading to pure materials combined with their suitability as luminescent materials makes the title compounds worthy candidates to be considered for further investigation regarding technical phosphor application.

Acknowledgment

The authors thank Dr. Sabine Strobel for measuring the diffuse reflectance spectra with the fluorescence spectrometer of Prof. Dr. Wolfgang Kaim (Institute for Inorganic Chemistry, University of Stuttgart, Germany) and Dipl.-Chem. Florian Ledderboge for measuring the single-crystal Raman spectra with the vibration spectrometer of Prof. Dr. Hans-Joachim Massonne (Institute for Mineralogy and Crystal Chemistry, University of Stuttgart, Germany). Furthermore, the financial support by the State of Baden-Württemberg (Stuttgart, Germany) and the Fonds der Chemischen Industrie (Frankfurt am Main, Germany) is gratefully acknowledged.

References

[1] L.H. Brixner, H.-Y. Chen, C.M. Foris, J. Solid State Chem. 45 (1982) 80–87.
[2] L.H. Brixner, H.-Y. Chen, C.M. Foris, Mater. Res. Bull. 17 (1982) 1545–1556.
[3] Th. Schleid, S. Strobel, P.K. Dorhout, P. Nockemann, K. Binnemans, I. Hartenbach, Inorg. Chem. 47 (2008) 3728–3735.
[4] I. Hartenbach, S. Strobel, Th. Schleid, K.W. Krämer, P.K. Dorhout, Z. Anorg. Allg. Chem. 635 (2009) 966–975.
[5] I. Hartenbach, Th. Schleid, S. Strobel, P.K. Dorhout, Z. Anorg. Allg. Chem. 636 (2010) 1183–1189.
[6] T. Schustereit, Doctoral Thesis, University of Stuttgart, 2015.
[7] G. Blasse, B.C. Grabmeier, Luminescent Materials, Springer-Verlag, Berlin, Heidelberg, 1994.
[8] S. Laufer, S. Strobel, Th. Schleid, J. Cybinska, A.-V. Mudring, I. Hartenbach, New J. Chem. 37 (2013) 1919–1926.
[9] A.M. Kaczmarek, K. van Hecke, R. van Deun, Inorg. Chem. 53 (2014) 9498–9508.
[10] X.C. Yu, Y.B. Qin, M.L. Gao, L. Duan, Z.Q. Jiang, L. Gou, P. Zhao, Z. Li, J. Lumin. 153 (2014) 1–4.
[11] WinXPOW: Program for Adaption and Analysis of Powder Patterns (version 3.04), Fa. Stoe, Darmstadt, Germany, 2010.

[12] W. Herrendorf. H. Bärnighausen. HABITUS: Program for the Optimization of the Crystal Shape for Numerical Absorption Correction in X-SHAPE (Version 1.06). Fa. Stoe, Darmstadt, Germany, Karlsruhe, Gießen, Germany, 1993, 1996, 1999.
[13] G.M. Sheldrick, Acta Crystallogr. A 64 (2008) 112–122.
[14] Th. Hahn, A.J.C. Wilson, second ed.,International Tables for Crystallography, vol. C, Kluwer Academic Publishers, Boston, MA, 1992.
[15] R. Hoppe, Adv. Fluorine Chem. 6 (1970) 387–438.
[16] R. Hoppe, Izv. Jugoslav. Centr. Krist. 8 (1973) 21–36.
[17] R. Hoppe, Crystal Structure and Chemical Bonding in Inorganic Chemistry, in: C.J.M. Rooymans, A. Rabenau (Eds.), North-Holland Publishing Company, Amsterdam, 1975, pp. 127–161.
[18] R. Hoppe, Angew. Chem. Int. Ed. Engl. 19 (1980) 110–125.
[19] G. Kortüm, Reflectance Spectroscopy, Springer, Berlin, New York, 1969.
[20] N.J. Yamashita, Phys. Soc. Jpn 35 (1973) 1089–1097.
[21] W.W. Wendlandt, H.G. Hecht, Reflectance Spectroscopy, Interscience Publishers, New York, NY, 1966.
[22] G.H. Dieke, Spectra and Energy Levels of Rare Earth Ions in Crystals, Interscience Publishers, New York, NY, 1969.
[23] W. Bo, M. Zinkevich, F. Aldinger, W. Dingzhong, C. Lu, J. Solid State Chem. 180 (2007) 3280–3287.
[24] I. Hartenbach, S. Jagiella, Th. Schleid, J. Solid State Chem. 179 (2006) 2258–2264.
[25] Th. Schleid, G. Meyer, Z. Kristallogr. 210 (1995) 145.
[26] M. Gärtner, D. Abeln, A. Pring, M. Wilde, A. Reller, J. Solid State Chem. *111* (1994) 128–133.
[27] G. Busca, J. Raman Spectrosc. 33 (2002) 348–358.
[28] M. Daub, A.J. Lehner, H.A. Höppe, Dalton Trans. 41 (2012) 12121–12128.
[29] R. van Deun, K. Binnemans, C. Görller-Walrand, J.L. Adam, J. Alloys Compd. 283 (1999) 59–65.
[30] G. Blasse, G.J. Dirksen, Mater. Chem. Phys. 21 (1989) 293–299.